Image Processing for Kidney Stone Segmentation and Surface Area Estimation Using CT Scans

Zuhier Humady Hussien[1,2], Rabab Saadoon Abdoon[1] and Nihad Abdulameer Salih[1]
[1]*Department of Physics, Faculty of Science, University of Babylon, 51002 Babylon, Iraq*
[2]*Al-Furat Al-Awsat Hospital, Najaf Health Directorate, Iraqi Ministry of Health, 54001 Najaf, Iraq*
sci753.zuhair.hamadi@student.uobabylon.edu.iq, sci.rabab.saadoon@uobabylon.edu.iq, sci.nihad.abdul@uobabylon.edu.iq

Keywords: Kidney Stone Fragmentation, Helical Computed Tomography(CT), Pre-Image Filtering, Image Segmentation, K-Means, FCM, Contrast Adjustment, ESWL, MATLAB, Image Enhancement.

Abstract: This study presents an integrated image-processing framework for kidney stone segmentation and surface area estimation from helical CT scans to support ESWL treatment planning. The proposed approach combines pre-processing (Prewitt, Laplacian, and sharpening filters), segmentation methods (K-means clustering and Fuzzy C-Means), and contrast enhancement to improve stone visibility in noisy, low-contrast CT images. Image quality was evaluated using MSE, PSNR, and SSIM metrics, while segmentation accuracy was validated by comparing automatically extracted stone areas with expert urologist annotations. Experiments were conducted on 10 clinically selected CT cases (5 fragmentable and 5 non-fragmentable stones). Results show that Prewitt and sharpening filters provide improved edge preservation and structural similarity, while K-means (k = 4, 5) and FCM effectively segment stone regions under varying contrast conditions. The proposed framework achieved strong agreement with expert measurements, with most surface area deviations below 5%. Overall, the results demonstrate that combining classical filtering, clustering, and contrast enhancement significantly improves kidney stone localization and quantification. The method is clinically reliable for ESWL planning, though performance decreases for very small stones (<20 pixels), indicating a need for further refinement in low-resolution cases.

1 INTRODUCTION

One of the most important causes of kidney stones is an imbalance in the chemical composition of urine. Another cause is an imbalance in food metabolism. This metabolic imbalance refers mainly to increased urinary concentration of minerals and salts—such as uric acid, calcium, oxalate, and phosphate —beyond their solubility limits, Crystal formation and accumulation occur when urine becomes saturated with these components, leading to the formation of a renal stone [1]. Kidney stones of various sizes are considered a prevalent urological disorder caused by the accumulation of crystalline materials in the urinary system (kidneys, ureters, or bladder) [2]. Extracorporeal Shock Wave Lithotripsy (ESWL) is considered one of the most important methods used for stones under 25 mm. The ESWL device employs focused electrohydraulic or piezoelectric shock waves that pass through living tissue and It focuses on the stone and causes it to break down, causing its fragmentation into small particles that can be excreted naturally with urine. There are several ways to locate the stone, including using ultrasound or fluoroscopic imaging, ensuring effective fragmentation and This helps reduce tissue damage. Due to an inaccurate location. High-definition localization to ensure complete fragmentation and avoid damage to tissues near the stone [2].Due to its high accuracy, CT scanning is used to locate the stonedue to its high accuracy, image quality may be compromised by noise (such as Gaussian, Poisson, and speckle) and artifacts (e.g., patient motion and beam hardening) [3]. When using an ESWL device, it is very important to improve the CT image.to treatment planning and ensuring accurate diagnosis.

Each filter performs a specific task in improving image quality:

1) The Prewitt filter emphasizes intensity gradients. Which helps to detect the edges in the image..

2) The Laplacian filter enhances fine structural details. This happens through Rapid intensity transitions using second-derivative calculations.
3) The Sharpened filter works to increase edge contrast by amplifying high-frequency components [4], [5].

All selected filters for their complementary strengths in improving edge visibility and structural detail before segmentation. Their theoretical characteristics guided the enhancement stage of this study. Although filters such as Laplacian, Prewitt, and sharpening also help to enhance edge visibility, they may not always preserve critical anatomical details [4], [6], [7]. Fuzzy C-Means (FCM) clustering is quite widely applied in medical image segmentation. This is because it allows each pixel to belong to multiple clusters with varying degrees of membership. This soft classification capability improves the representation of gradual transitions in CT images, and it helps solve many problems, including the problem of overlapping tissue intensities and low-contrast boundaries. These are problems that are repeated in imaging kidney stones [8], [9].

This is to achieve good results in accurate stone detection. The study evaluates three segmentation methods, and it is: K-means clustering with k values of 4 and 5 to classify pixels according to their density [10].

Second, Fuzzy C-Means (FCM) clustering Technology was used to manage cases with unclear or overlapping boundaries. Fuzzy C-Means (FCM), which allows for soft sorting, is useful for indistinct boundaries and contrast adjustment for greater clarity and highlighting stones in low-contrast images [11].

For clinical verification, urologist Dr. Muthanna Habib Al-Athari performed. where he drew diagrams around the outer borders of the stone; both fragmentable (F) and non-fragmentable (NF) stones on CT images were generated to be a reliable reference for comparing all results for subsequent algorithmic comparisons.

Several CT scans were collected from the urology departments in hospitals in Najaf Governorate, including Al-Sadr Teaching Hospital and Al-Furat Al-Awsat Teaching Hospital. Ethical approvals were obtained from the Najaf Health Department. Health Directorate, and the requirement for individual patient consent was waived. To ensure patient anonymity, all information and data from the images used in the research were removed. The cohort exclusively included Cases with a new diagnosis of kidney stones and no history of prior surgical or medical intervention for this condition. For scientific documentation, all scans were acquired per standard clinical protocols between January 2023 and March 2024.

This study was designed to achieve the following objectives:

1) Working on improving CT image clarity through a dedicated pipeline for edge definition and external borders contrast improvement.
2) To develop and validate an accurate methodology for stone surface segmentation and accurately measure the area of the stones.
3) To rigorously evaluate the clinical reliability of the automated Compare it to the results by benchmarking them against expert urologist annotations.

2 MATERIALS AND METHODS

This study employed MATLAB (version 2016). All image processing commands of this program are used in segmentation and enhancement tasks. A dataset of 24 helical CT images of kidney stones was analyzed. These images were obtained from patients who were confirmed to have kidney stones. The images were acquired using a Siemens SOMATOM, which is a type of helical CT scanner with a slice thickness of 1 mm. From this set, Selected by a urologist selected 5 cases classified as fragmentable and 5 as non-fragmentable, ensuring clinical relevance and consistency throughout the evaluation process. All this data has been collected and verified from clinical sources, and it was not collected from a public database.

2.1 Workflow of the Proposed Method

This flowchart represents a detailed explanation of the work, in order to standardize and visualize the analysis process (Fig. 1). This is a plan that outlines. It explains each stage of the work, including photo collection, expert classification, enhancing photos with filters, using the three fragmentation methods, and working to get the final evaluation. The integration of automated analysis with clinical expertise helps ensure both methodological robustness and medical relevance.

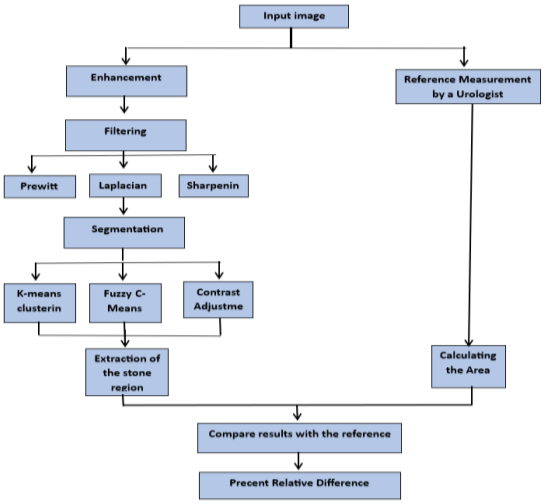

Figure1: Methodology for kidney stone segmentation and evaluation in ESWL planning.

2.2 Filtering Techniques

To improve kidney stone visibility before segmentation, three pre-processing filters were applied: Laplacian, Prewitt, and Sharpened filters [11]. As shown in the following two Figures 2, 3. To indicate the presence of the stone,a red circle was added to distinguish it before applying the enhancement and filtering techniques.This visual marker facilitates a more accurate comparison among the different filtering methods.

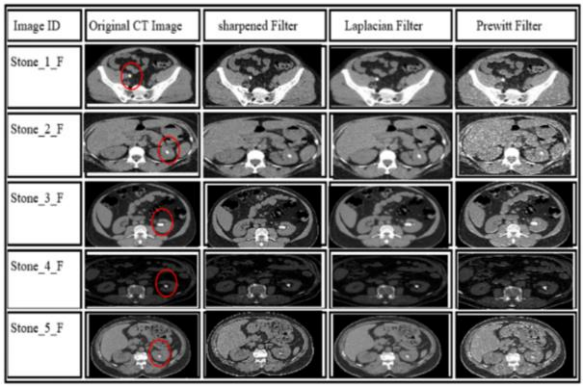

Figure 2: Filtered CT images of 5 kidney stones suitable for fragmentation using three filters (Prewitt, Laplacian, and Sharpened) before segmentation.

2.3 Segmentation Methods

The segmentation process is one of the most important steps used to separate stones from the surrounding tissue and bone in the anatomical structure of spiral CT images [12]. This allows for accurate measurement of stone areas.which helps in assessing the suitability of these stones for fragmentation with shock waves [3], [13].In this study, three segmentation methods were performed on images selected after pre-filtering for both fragmentable and non-fragmentable stone types.: K-means clustering, Fuzzy C-Means (FCM), and contrast adjustment.

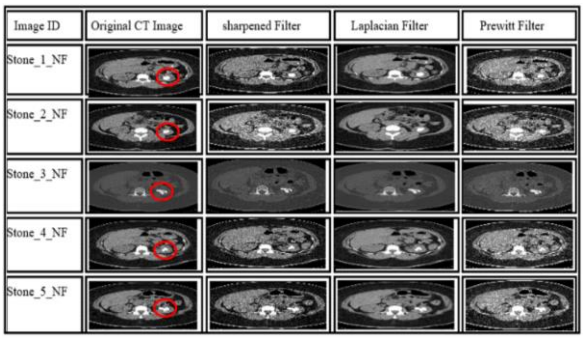

Figure 3: Filtered CT images of 5 kidney stones unsuitable for non-fragmentation using Prewitt, Laplacian, and sharpened filters before segmentation.

2.3.1 K-means Clustering

K-means clustering. This type of clustering helps classify each pixel of the image into known clusters (k) based on the intensity level. It is considered an unsupervised approach that aids in distinguishing between kidney stones and surrounding tissues [11]. Two cluster counts (k = 4, 5) were used in this investigation to define the image boundaries and clarify the segmentation process [14]:

1) k=4: to improve boundary sharpness, especially in low-contrast regions.
2) k=5: Get more detailed segmentation by highlighting subtlety and nuance intensity differences [15].

The following Figures 4-7 illustrate the application of K-means clustering to filtered images. K-means clustering of CT scans from both types of stones used in the research, using the tested k-values, demonstrating its effectiveness in supporting ESWL planning, additional processing steps were applied to enhance the accuracy of the segmentation results.

This included thresholding, removing, and filling internal gaps, and getting rid of small and isolated spaces. This refinement helped improve boundary precision and surface area calculation, ensuring robust quantitative analysis.

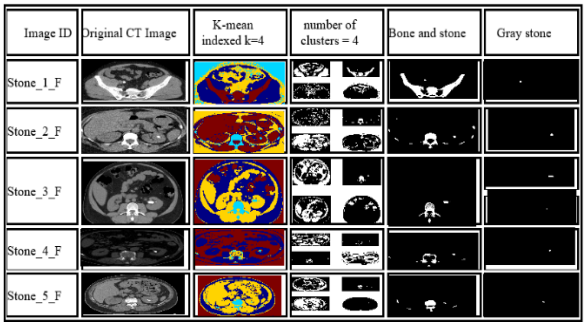

Figure 4: Image results after segmentation, using K-means clustering when k=4, for 5 fragmentable kidney stones after pre-filtering.

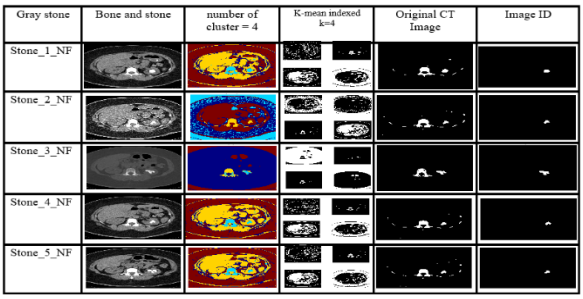

Figure 5: Image results after segmentation, using K-means clustering when k=4, for 5 non-fragmentable kidney stones after pre-filtering.

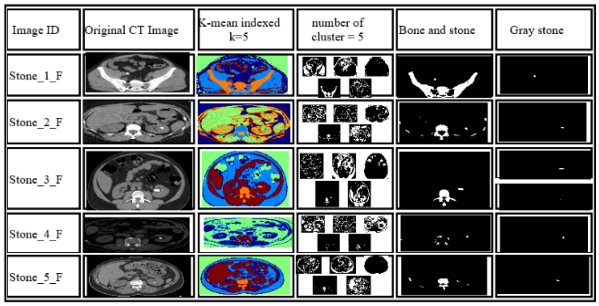

Figure 6: Image results after segmentation, using K-means clustering when k=5 for 5 fragmentable kidney stones after pre-filtering.

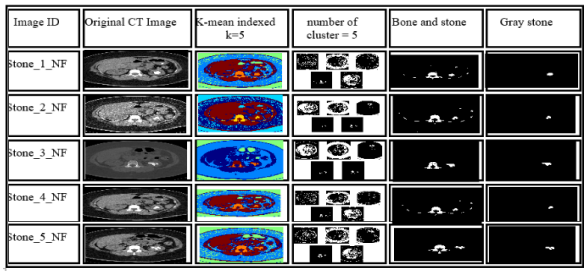

Figure 7: Image results after segmentation, using K-means clustering when k=5 for 5 non-fragmentable kidney stones after pre-filtering.

2.3.2 Fuzzy C-Means (FCM) Clustering

The Fuzzy C-Means (FCM) clustering algorithm was used to deal with unclear cases, and the real handling of overlapping or indistinct boundaries. This helps to provide soft segmentation of kidney stones in low-contrast CT images.

FCM effectively manages uncertainty by assigning pixels partial memberships across clusters, which further enhances the segmentation of low-contrast or overlapping regions. However, its iterative membership updates increase computational demand and sensitivity to the initial membership matrix, which may lead to local minima or unstable results [8], [9].

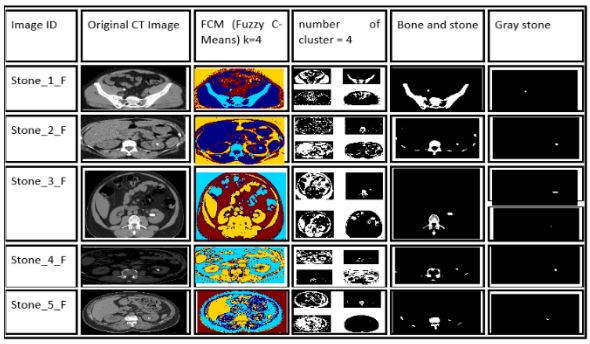

Figure 8: Segmentation results using Fuzzy C-Means (FCM) clustering with k=4 for five fragmentable kidney stones after pre-filtering.

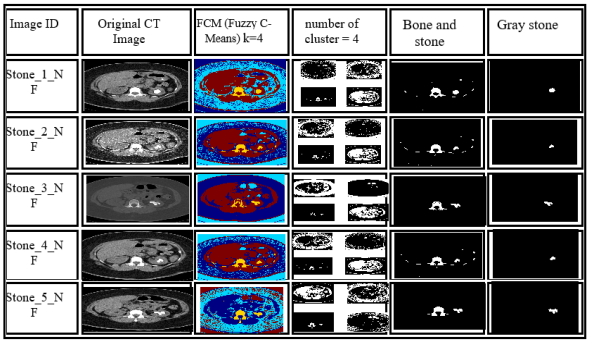

Figure 9: Segmentation results using Fuzzy C-Means (FCM) clustering with k=4 for five non-fragmentable kidney stones after pre-filtering.

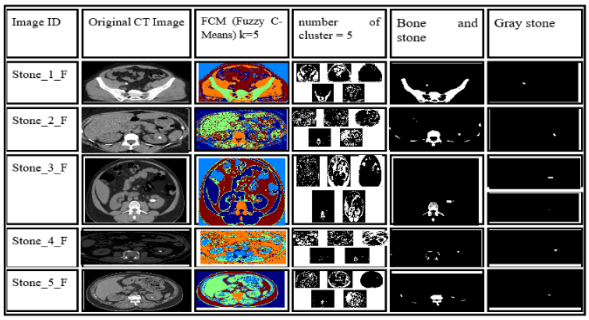

Figure 10: Segmentation results using Fuzzy C-Means (FCM) clustering with k=5 for five fragmentable kidney stones after pre-filtering.

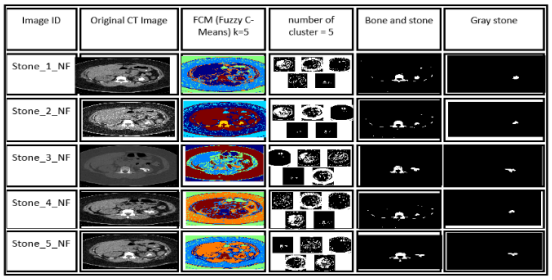

Figure 11: Segmentation results using Fuzzy C-Means (FCM) clustering with k=5 for five non-fragmentable kidney stones after pre-filtering.

Figures 8-11 display FCM segmentation results for different cluster values. To evaluate its segmentation performance across varying image complexities and different contrast conditions, FCM was applied in this study to CT images that had been previously processed with filtering techniques:

1) To make a necessary comparison with K-means results, more than one value was taken: Cluster count (k = 4,5).
2) Membership thresholding. Used to generate binary segmentation masks. by isolating pixels with high membership values [16], [17].
3) Morphological filtering. Where there are several sequential processes, including operations like getting rid of unnecessary spaces and hole filling [8], [18], [19].To refine the segmentation masks.

Segmentations were then used to calculate stone surface areas and compared against expert urologist annotations for validation [20].

2.3.3 Contrast Adjustment

This method plays a crucial role in enhancing the clarity of kidney stones in the images, especially when the intensities of the stones and the surrounding areas are close in value, as is often the case in low-contrast or isointense CT images, In such cases, this technique effectively modifies the pixel intensity distribution [17], [21]. In such cases, this technique effectively modifies the pixel intensity distribution, which occurs by stretching the histogram, which amplifies the contrast between the stone and surrounding structures while suppressing background interference [15], [22].

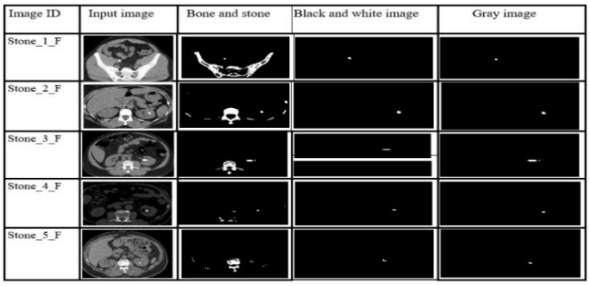

Figure 12: Contrast-adjusted CT images of five fragmentable kidney stones.

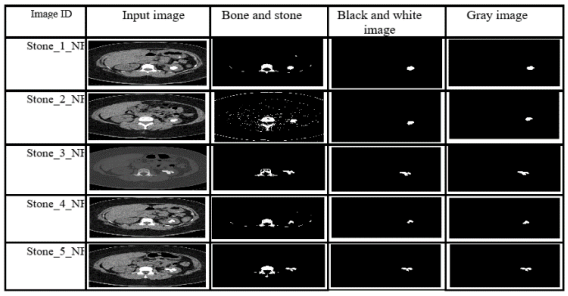

Figure 13: Contrast-adjusted CT images of five non-fragmentable kidney stones.

In Figures 12 and 13, the initial filtration process was carried out, followed by contrast enhancement. This step is important for improving the delineation of stone edges. To ensure that the optimization process runs smoothly, binary masks were created, performing morphological operations like hole filling, noise elimination, and calculating the actual area of the stones.

The results confirmed that contrast adjustment makes an effective contribution to clearer boundary definition and a more accurate estimate. To evaluate the effectiveness of this work scientifically and logically, the resulting segmented areas were compared to manually annotated references manually selected by a urology specialist, reinforcing its clinical significance in planning extracorporeal shock wave lithotripsy (ESWL) procedures.

2.4 Reference Measurement by Urologist

To evaluate the accuracy of segmentation outcomes, A standard has been set through a manual procedure conducted by an experienced urologist, as follows:

1) Select image and Preparation. Ten spiral CT scan images showing kidney stones were used. (five fragmentable and five non-fragmentable) were printed for clarification.
2) Place a transparent film over the printed image. A transparent sheet with a thickness of 0.125 mm, Paper size A4 placed over each printed image, Manual Boundary Annotation: Using a special fine-tipped highlighter pen, the urologist drew carefully the kidney stone boundaries while excluding adjacent structures.
3) Scanning of Annotations. Using the scanner, the required images were scanned.
4) Digital Processing of the Annotations. Kidney stones are filled with white color and a black background to create binary images.
5) Surface Area Extraction. These binary masks were analyzed using the same computational pipeline applied to automated segmentations, which helped to measure the surface area well. These expert-drawn annotations served as the ground truth reference against which automated surface area estimations were evaluated.
6) To ensure the reliability of the manually delineated reference, the annotations were reviewed accurately by the same urologist with a one-week interval to minimize intra-observer variability. In addition, ambiguous boundaries have been carefully verified against the original digital CT images before digitization. This procedure ensured consistency and minimized subjectivity in the ground truth creation process.

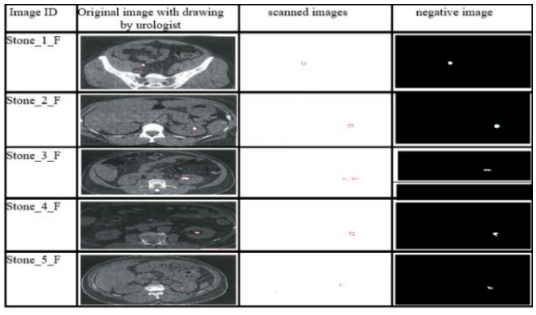

Figure 14: Physician-annotated contours of five fragmentable kidney stones on helical CT images,

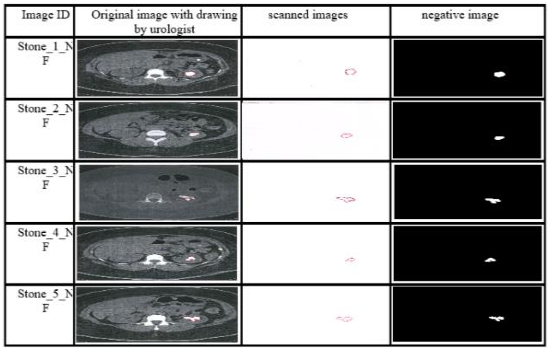

Figure 15: Physician-annotated contours of five non-fragmentable kidney stones on helical CT images,

As shown in Figures 14, 15, the physician-generated contours visibly define the stone boundaries and form the basis for evaluating the performance of automated segmentation.

While the manually derived surface areas were compared to those generated by automated methods (K-means, FCM, contrast adjustment), and a relative percentage difference (PRD) was calculated to quantify agreement, The manually drawn contours were treated as the ground truth and used as the clinical benchmark to validate the segmentation methods.

3 RESULTS

3.1 Outcomes of K-means Clustering

The K-means algorithm showed strong segmentation performance, particularly at k=4, where it effectively distinguished stones, soft tissue, and background in most cases, especially in small areas of kidney stones that are difficult to separate Figures 4, 5. When the number of groups increases to k=5, enhanced edge clarity, particularly in low-contrast conditions Figures 6, 7. Overall, a higher k enhanced segmentation accuracy but slightly increased computational.

3.2 Outcomes of Fuzzy C-Means (FCM) Clustering

FCM clustering was tested at k=4,5, demonstrating variable performance based on contrast level and stone type, as well as in addition to its size and location. When k=4, FCM effectively segmented fragmentable and non-fragmentable stones as shown in Figures 8, 9. At k=5, better results were obtained for fragmentable stones. And so it was, good results

were obtained for non-fragmentable stones. And also Figures 10, 11. These outcomes suggest that FCM is well-suited for high-contrast regions and small spaces, but it has difficulty in anatomically complex regions near bone.

3.3 Contrast Adjustment Results

Contrast enhancement notably improved visibility and segmentation in the vast majority of fragmentable stones (Fig. 12), leading to more accurate area measurement. This method is characterized by high accuracy and ease of implementation. In non-fragmentable stones (Fig. 13), the improvement was moderate, particularly near iso-dense bone zones, which required sequential post-processing. Overall, contrast adjustment contributed to better segmentation outcomes when integrated with clustering techniques [23]. which contributed to an increase in improvement for using ESWL planning.

3.4 Evaluation of Filtering Techniques Using MSE, PSNR, and SSIM

To assess the influence of filters on image clarity before segmentation, three standard metrics were employed:

Mean Squared Error (MSE). This type of scale measures the average squared difference between the original image and the filtered image, as in Equation (1). As the decrease in MSE suggests less distortion and higher similarity [20], [24].

$$2[K(i,j) - I(i,j)] \sum_{j=0}^{n-1} \sum_{i=0}^{m-1} \frac{1}{mn} = MSE, \quad (1)$$

where I (i, j) and K (i, j) refer to the pixel values of the original and filtered images, In succession. Lower MSE indicates greater symmetry and less distortion. Peak Signal-to-Noise Ratio (PSNR) measures image quality relative to noise[24].

$$\left(\frac{I^2\, MAX}{MSE}\right) 10 \log .10 = PSNR\,, \quad (2)$$

where IMAX is the maximum pixel value. Higher PSNR values reflect better image quality [25].
Structural Similarity Index Measure (SSIM) evaluates perceived image quality by comparing luminance, contrast, and structure between images, as shown in (3) as [19], [26]:

$$\frac{\left(2^2\sigma xy + C\right)\left(1^2\mu\chi\mu\Upsilon + \mathrm{C}\right)}{\left(2\sigma_\chi^2 + \sigma_\Upsilon^2 + \mathrm{C}\right)\left(1\mu_\chi^2 + \mu_y^2 + \mathrm{C}\right)} = SSIM(\chi,\gamma), \quad (3)$$

where μ and σ are means and standard deviations, respectively, and C is a stabilizing constant. SSIM ranges from (-1 to 1), with values closer to 1, which means high structural similarity[27], [28].

Three highly selected types of filters were tested: Prewitt (for edge emphasis), Laplacian (to capture rapid intensity shifts), and Sharpened (for enhancing fine structures).

Table 1: Image quality evaluation (MSE, SSIM, PSNR) of enhanced filters versus original CT images for five fragmentable stones.

Image	Methods								
	Laplacian Filtered			Prewitt filtered			Sharpened Filter		
	MSE	SSIM	PSNR	MSE	SSIM	PSNR	MSE	SSIM	PSNR
Stone_1_F	12490.6	0.188	7.164	13757.9	0.129	6.745	8907.6	0.511	8.633
Stone_2_F	11531.8	0.062	7.511	10007.7	0.043	8.127	12397.6	0.368	7.197
Stone_3_F	6151.1	0.178	10.24	5560.4	0.241	10.67	9255.3	0.519	8.466
Stone_4_F	1334.4	0.287	16.87	1197.1	0.320	17.34	4150.3	0.517	11.95
Stone_5_F	6218.1	0.020	10.19	5460.3	0.157	10.75	10607.1	0.573	7.874

Table 2: The table shows which filters applied to the Input image are best. The comparison is done using the following variables (MSE, SSIM, PSNR) of five fragmentable kidney stones.

Image number	The best (MSE)	The best (PSNR)	The best (SSIM)
Stone_1_F	sharpened	sharpened	sharpened
Stone_2_F	Prewitt	Prewitt	sharpened
Stone_3_F	Prewitt	Prewitt	sharpened
Stone_4_F	Prewitt	Prewitt	sharpened
Stone_5_F	Prewitt	Prewitt	sharpened

Table 3: Image quality evaluation (MSE, SSIM, PSNR) of enhanced filters versus original CT images for five non-fragmentable stones.

Image	Methods								
	Laplacian Filtered			Prewitt filtered			Sharpened Filter		
	MSE	SSIM	PSNR	MSE	SSIM	PSNR	MSE	SSIM	PSNR
Stone_1_NF	6823.906	0.074	9.790	6117.785	0.187	10.264	8046.176	0.486	9.074
Stone_2_NF	6243.507	0.060	10.176	5651.335	0.198	10.609	7677.300	0.485	9.278
Stone_3_NF	4304.354	0.142	11.791	3946.973	0.173	12.168	15715.726	0.568	6.167
Stone_4_NF	7010.900	0.081	9.673	6278.084	0.190	10.152	8184.871	0.487	9.0006
Stone_5_NF	6588.652	0.072	9.942	5972.214	0.189	10.369	7796.586	0.490	9.211

Table 4: The table shows which filters applied to the Input image are best. The comparison is done using the following variables (MSE, SSIM, PSNR) of five non-fragmentable kidney stones.

Image number	The best (MSE)	The best (PSNR)	The best (SSIM)
Stone_1_NF	Prewitt	Prewitt	sharpened
Stone_2_NF	Prewitt	Prewitt	sharpened
Stone_3_NF	Prewitt	Prewitt	sharpened
Stone_4_NF	Prewitt	Prewitt	sharpened
Stone_5_NF	Prewitt	Prewitt	sharpened

Through pre-selected CT scan images, all filters were applied with high precision to each image separately. To make sure that the performance of each of them is measured against the original scans using three quality measures: MSE, PSNR, and SSIM metrics. The results obtained were included in the Tables 1 and 3, where each table shows a clear and concise comparative summary of how each filter sharing to image quality and anatomical clarity.

3.5 Evaluation and Analysis of Filters

Three types of filtration techniques were studied and quantitatively evaluated as follows: Laplacian, Prewitt, and Sharpened - using the image quality metrics mentioned formerly: Mean Squared Error (MSE), Peak Signal-to-Noise Ratio (PSNR), and Structural Similarity Index Measure (SSIM). Tables 1 and 2 represent the fragmentable stone group. For (MSE), the best results for the five images were as follows: (5460.313, 4150.278, 5560.356, 10007.798, and 8907.627), respectively. As for (SSIM), the best results that could be obtained were: (0.573, 0.517, 0.519, 0.368, and 0.511) respectively. As for (PSNR), the search results were as follows, in order: (10.758, 17.349, 10.679, 8.127, and 8.633).

Both the Sharpened and Prewitt filters outperformed the Laplacian filter, as indicated by reduced MSE values and improved PSNR scores. The Sharpened filter delivered the largest values of SSIM scores in most cases of images. indicating superior structural preservation. The research has concluded that the Prewitt filter values achieved results in MSE and PSNR, highlighting that this gives an idea of overall robustness.

For non-fragmentable stones (Tables 3 and 4), for (MSE), the best results for the five images were as follows: (6117.785, 5651.335, 3946.973, 6278.084, 5972.214) respectively. As for (SSIM), the best results that could be obtained were: (0.486, 0.485, 0.568, 0.487, 0.490) respectively. As for (PSNR), the results were as follows, in order: (10.264, 10.609, 12.168, 10.152, 10.369). The Prewitt filter again demonstrated consistent superiority in MSE and PSNR, especially in difficult low-contrast cases. At the same time, the Sharpened filter maintained the lead in SSIM, which gives an idea about its ability to preserve image structure under challenging conditions, filter yielded the highest image quality (MSE = 3946.97, SSIM = 0.173, PSNR = 12.17), followed by the Laplacian filter (MSE = 4304.35, PSNR = 11.79), while the Sharpened filter showed superior structural similarity (SSIM = 0.568) but lower PSNR values. These findings confirm that Prewitt filtering provided the most balanced enhancement between noise suppression and edge preservation.

After the filtration process and using three methods, the segmentation process was carried out: K-means, FCM, and contrast adjustment. The comparison resulted in surface area measurements. Compared with the work of a urologist, annotations to validate the clinical reliability of each method across both stone types, fragmentable and non-fragmentable.

3.6 Surface Area Measurement and Comparison

To assess the precision of the segmentation techniques, surface area measurements of kidney stones were extracted using the three fragmentation methods: K-means, Fuzzy C-Means (FCM), and contrast adjustment [21], [24] These values were then compared against manual annotations performed by a urologist. As detailed in Tables 5, 6.

The results are shown in Table 5, which concerns the Surface Area of Fragmentable Stones, with high consistency with the urologist's manual delineation. For instance, in Stone_1_F, the reference value was 168 px, while the results ranged between 159 and 163 Pixel. This represents a slight difference. On the other hand, in Stone_2_F (195 Pixel), the three ways yielded values between 186–191 Pixel, and for Stone_3_F (252 Pixel), the results were within 244–255 Pixel. From the previous results, we conclude that there is a high level of agreement. Other differences across all stones were within a slight range (±5–10 Pixel), which confirms that the results were accurate and reliable. of the applied segmentation techniques.

Automated segmentation methods for non-fragmentable stones in Table 6 yield good results, highly close to the urologist's delineation, with differences generally within 3–5%. K-means and FCM maintained close agreement across all cases, while contrast adjustment showed slightly greater differences than other methods in variation in Stone_1_NF.

To quantify the variation between the automated and manual measurements, the Percent Relative Difference (PRD) was calculated according to (4) [23].

$$PRD = \left|\frac{A_{mehad} - A_{reference}}{A_{reference}}\right| \times 100\ \%. \quad (4)$$

Where: *A method* is the automatically calculated stone area, *A reference* is the area annotated by the urologist [25].

When comparing the results, we obtained using the three methods with the results of the urologist, as in the Table 7, for Fragmentable Stone, and calculating the percentage, we notice that segmentation accuracy remained close to the urologist's reference, with most deviations ranging between 1–5%, with very few results deviating slightly from this range Stones 1–3 demonstrated minimal variation, indicating high-resolution performance across different cluster settings.

For Stone_4_F, the results were different, particularly in some clustering cases where values dropped to zero. Stone_5_F also showed slightly different results. And Exceptions occurred in stones <20 pixels, where segmentation is more sensitive to small errors due to limited resolution and partial volume effects. All the results confirm that the applied methods generally maintained acceptable agreement with clinical delineations.

Table 5: Surface area (pixels) of fragmentable stones, comparison of segmentation methods with urologist reference.

Images	Four		Five		Contrast adjustment	Urologist delineation
	K-means	FCM	K-means	FCM		
Stone_1_F	163	160	160	159	160	168
Stone_2_F	187	187	186	186	191	195
Stone_3_F	255	251	253	254	248	252
	15	14	15	14	16	15
Stone_4_F	181	173	179	176	169	176
Stone_5_F	79	76	78	73	76	76

Table 6: Surface area (pixels) of non-fragmentable stones, comparison of segmentation methods with urologist reference.

Images	Four %		Five %		Contrast adjustment	Urologist Delineation
	K-means	FCM	K-means	FCM		
Stone_1_NF	1122	1126	1116	1114	1086	1137
Stone_2_NF	877	842	865	862	887	859
Stone_3_NF	1351	1351	1350	1393	1383	1386
Stone_4_NF	772	772	768	768	819	784
Stone_5_NF	1150	1159	1158	1152	1147	1157

Table 7: Percentage difference in surface area estimation compared with urologist reference (fragmentable stones).

Images	Four		Five		Contrast adjustment
	K-means	FCM	K-means	FCM	
Stone_1_F	2.97	4.76	4.76	5.35	4.76
Stone_2_F	4.10	4.10	4.61	4.61	2.051
Stone_3_F	1.98	0.39	0.39	0.79	1.58
	0	6.66	0	6.6	6.66
Stone_4_F	2.84	1.70	1.70	0	3.97
Stone_5_F	3.94	0	2.63	0	0

Table 8:Percentage difference in surface area estimation compared with urologist reference (non-fragmentable stones).

Images	Four %		Five %		Contrast adjustment
	K-means	FCM	K-means	FCM	
Stone_1_NF	1.31	2.022	1.84	2.022	4.48
Stone_2_NF	2.09	1.97	0.69	0.34	3.25
Stone_3_NF	2.52	2.52	2.59	0.50	0.21
Stone_4_NF	1.53	1.53	2.020	2.040	4.46
Stone_5_NF	0.605	0.17	0.086	0.43	0.86

Table 8 Shows the percentage differences in surface area estimation for non-fragmentable stones, Which were compared with the results obtained from the doctor's results. Most deviations remained within a narrow range of 0.08% to 4.5%. indicating a high degree of performance. The biggest differences were in the outcome Stone_1_NF. while the rest of the stones showed much closer agreement, confirming the reliability of the applied segmentation methods even under challenging imaging conditions.

4 DISCUSSION

This study introduced an integrated Process combining Laplacian ,Prewitt, and sharpened filters with K-means, FCM clustering, and contrast adjustment to get the best result in kidney stone detection and surface area estimation in helical CT images for ESWL planning.

4.1 Segmentation Performance

K-means clustering has proven its high efficiency in segmentation, with k = 4 offering an effective trade-off between preserving structural detail and minimizing noise. The increase in the number of groups was to k = 5. This is quite clear in the precision of the demarcation of the borders, especially in complex cases.FCM made a technique that provided flexible segmentation in transitional regions but showed reduced performance near bone interfaces in non-fragmentable, low-contrast images. Contrast enhancement consistently this improvement contributed to the overall image On the other hand, particularly in low-contrast or iso-dense conditions. Expanding the dynamic range of pixel intensities facilitated more distinct boundary identification, complementing the effectiveness of both K-means and FCM segmentation strategies.

4.2 Edge Detection and Filtering

Edge enhancement using sharpened and Prewitt filters significantly improves the ability to distinguish and identify edges with higher capabilities than before, stone contour vision, and observation by reinforcing intensity gradients and suppressing background noise. These filters have contributed to and helped in more accurate mask generation and clearer separation of kidney stones from adjacent anatomical structures.

4.3 Evaluation of Segmentation Performance

The three measures used are shown. (MSE, SSIM, PSNR) showed excellent performance and superior results of Prewitt and sharpened filters over Laplacian in preserving the image while maintaining structure and accuracy. Automated surface area measurements closely matched and clearly urologist-defined references[20], with most PRD values under 5%, confirming clinical accuracy. Higher PRD in stones smaller than 20 pixels was attributed to segmentation sensitivity under resolution limitations.

These studies have shown that the proposed method significantly improved the accuracy of kidney stone localization and quantification in CT images, which contributed to developing a tool for

ESWL treatment planning. There are certain restrictions in dealing with small stones and the need for manual parameter tuning, which may affect reproducibility across datasets.

5 CONCLUSIONS

In this research work, recent filtering methods are utilized to establish the efficiency and benefit of a holistic method combining filtering processes with cluster-based image segmentation and contrast enhancement for accurate identification and quantification of kidney stones from helical CT images for ESWL treatment planning. The application of Prewitt and sharpen filters delivered more precise definitions for image edges, while approaches involving the K-means and FCM algorithms and contrast enhancement delivered reliable and precise segmentation outputs. On the other hand, MSE, PSNR, and SSIM analyses supported the enhancement of image quality. In addition to this, the measurements from various methods were found to be consistent with the measurements taken from the urologist with respect to surface area values, with differences being within 5% for the greater number of cases.

Although this particular approach showed a limited precision for stones measuring less than 20 pixels, on the whole, the framework was efficient for fragmentable and non-fragmentable stones and helped increase targeting precision while shortening the number of ESWL treatment sessions for the patient. In addition to this, the combination of this approach with various methods for image segmentation provides a possible platform for developing efficient future solutions with diminished reliance on human operators and decision-making. The results affirm the potential for implementing optimized image-processing approaches within the current lithotripsy treatment process and thus support the enhancement of treatment safety and efficiency.

REFERENCES

[1] X. Long, M. Huang, and H. Hu, “Revascularization may accelerate renal dysfunction in hypertensive patients with moderate atherosclerotic stenosis of renal arteries,” Medical Hypotheses, vol. 144, p. 110008, 2020.

[2] C. Türk et al., “EAU guidelines on interventional treatment for urolithiasis,” European Urology, vol. 69, no. 3, pp. 475-482, 2016.

[3] B. E. Knudsen, “Laser fibers for holmium: YAG lithotripsy: What is important and what is new,” Challenge, vol. 3, p. 6, 2019.

[4] R. C. Gonzalez, R. E. Woods, and S. L. Eddins, Digital Image Processing Using MATLAB, Pearson Education India, 2004.

[5] L. Yang et al., “Contrast enhancement boost improves the image quality of CT angiography derived from 80-kVp cerebral CT perfusion data,” BMC Medical Imaging, vol. 24, no. 1, 2024, , doi: 10.1186/s12880-024-01373-7.

[6] A. Hore and D. Ziou, “Image quality metrics: PSNR vs. SSIM,” in 2010 20th International Conference on Pattern Recognition, IEEE, 2010, pp. 2366-2369.

[7] J. Moreau et al., “Contrast quality control for segmentation task based on deep learning models-Application to stroke lesion in CT imaging,” Frontiers in Neurology, vol. 16, p. 1434334, 2025.

[8] G. Litjens et al., “A survey on deep learning in medical image analysis,” Medical Image Analysis, vol. 42, pp. 60-88, 2017.

[9] A. Pimpalkar, D. K. J. B. Saini, N. Shelke, A. Balodi, G. Rapate, and M. Tolani, “Fine-tuned deep learning models for early detection and classification of kidney conditions in CT imaging,” Scientific Reports, vol. 15, no. 1, p. 10741, 2025.

[10] D. Shen, G. Wu, and H.-I. Suk, “Deep learning in medical image analysis,” Annual Review of Biomedical Engineering, vol. 19, no. 1, pp. 221-248, 2017.

[11] R. Szeliski, Computer Vision: Algorithms and Applications, Springer Nature, 2022.

[12] D.-H. Jang et al., “Kidney, ureter, and urinary bladder segmentation based on non-contrast enhanced computed tomography images using modified U-Net,” Scientific Reports, vol. 14, no. 1, p. 15325, 2024.

[13] D. L. Pham, C. Xu, and J. L. Prince, “Current methods in medical image segmentation,” Annual Review of Biomedical Engineering, vol. 2, no. 1, pp. 315-337, 2000.

[14] Z. Wang, A. C. Bovik, H. R. Sheikh, and E. P. Simoncelli, “Image quality assessment: from error visibility to structural similarity,” IEEE Transactions on Image Processing, vol. 13, no. 4, pp. 600-612, 2004.

[15] M. Sezgin and B. Sankur, “Survey over image thresholding techniques and quantitative performance evaluation,” Journal of Electronic Imaging, vol. 13, no. 1, pp. 146-168, 2004.

[16] J. C. Bezdek, R. Ehrlich, and W. Full, “FCM: The fuzzy c-means clustering algorithm,” Computers & Geosciences, vol. 10, no. 2-3, pp. 191-203, 1984, , doi: 10.1016/0098-3004(84)90020-7.

[17] 17 F. Milletari, N. Navab, and S.-A. Ahmadi, “V-net: Fully convolutional neural networks for volumetric medical image segmentation,” in 2016 Fourth International Conference on 3D Vision (3DV), IEEE, 2016, pp. 565-571.

[18] R. C. Gonzalez, Digital Image Processing, Pearson Education India, 2009.

[19] A. K. Jain, Fundamentals of Digital Image Processing, 1989.

[20] N. C. Grossmann, F. Panthier, L. Afferi, P. Kallidonis, and B. K. Somani, “Measuring kidney stone volume – practical considerations and current evidence from the EAU endourology section,” Current Opinion in Urology, vol. 35, no. 4, 2025, , [Online]. Available: https://journals.lww.com/courology/fulltext/2025/07000/measuring_kidney_stone_volume___practical.4.aspx

[21] R. P. Marcus et al., “Detection and characterization of renal stones by using photon-counting–based CT,” Radiology, vol. 289, no. 2, pp. 436-442, Aug. 2018, , doi: 10.1148/radiol.2018180126.

[22] M. Lei, H. Wu, X. Lv, and X. Wang, “Condseg: A general medical image segmentation framework via contrast-driven feature enhancement,” in Proceedings of the AAAI Conference on Artificial Intelligence, 2025, pp. 4571-4579.

[23] Z. Zhang and U. Bagci, “Segmentation quality and volumetric accuracy in medical imaging,” arXiv: Computer Science, 2024, , [Online]. Available: https://arxiv.org/abs/2404.17742

[24] Q. Huynh-Thu and M. Ghanbari, “Scope of validity of PSNR in image/video quality assessment,” Electronics Letters, vol. 44, no. 13, pp. 800-801, 2008.

[25] L. Maier-Hein and B. Menze, “Metrics reloaded: Pitfalls and recommendations for image analysis validation,” arXiv.org, 2022.

[26] A. Breger et al., “A study on the adequacy of common IQA measures for medical images,” in Proceedings of the 2024 International Conference on Medical Imaging and Computer-Aided Diagnosis (MICAD 2024), Springer Nature Singapore, 2025, pp. 451-462.

[27] L. Kong, M. Huang, L. Zhang, and L. W. C. Chan, “Enhancing diagnostic images to improve the performance of the Segment Anything Model in medical image segmentation,” Bioengineering, vol. 11, no. 3, 2024, , doi: 10.3390/bioengineering11030270.

[28] Z. Wang and A. C. Bovik, “Mean squared error: Love it or leave it? A new look at signal fidelity measures,” IEEE Signal Processing Magazine, vol. 26, no. 1, pp. 98-117, 2009, , doi: 10.1109/MSP.2008.930649.

[29] Y. Xie et al., “Knowledge-based collaborative deep learning for benign-malignant lung nodule classification on chest CT,” IEEE Transactions on Medical Imaging, vol. 38, no. 4, pp. 991-1004, 2018.